

# From axial C-hedra to general P-nets

G. Nawratil

*Institute of Discrete Mathematics and Geometry & Center for Geometry and Computational Design, TU Wien, e-mail:  
nawratil@geometrie.tuwien.ac.at*

**Abstract.** We give a full classification of continuous flexible discrete axial cone-nets, which are called axial C-hedra. The obtained result can also be used to construct their semi-discrete analogs. Moreover, we identify a novel subclass within the determined class of (semi-)discrete axial cone-nets, whose members are named axial P-nets as they fulfill the proportion (P) of the intercept theorem. Known special cases of these axial P-nets are the smooth and discrete conic crease patterns with reflecting rule lines. By using a parallelism operation one can even generalize axial P-nets. The resulting general P-nets constitute a rich novel class of continuous flexible (semi-)discrete surfaces, which allow direct access to their spatial shapes by three control polylines. This intuitive method makes them suitable for transformable design tasks using interactive tools.

**Key words:** rigid-foldability, continuous flexibility, planar quad-surface, semi-discrete surface, cone-nets

## 1 Introduction

A planar quad-surface (PQ-surface) is a plate-and-hinge structure made of quadrilateral panels connected by rotational (R) joints in the combinatorics of a square grid. Such a surface is called *continuous flexible* (or *rigid-foldable* or *isometric deformable*) if it can be continuously transformed by a change of the dihedral angles only. In general a rigid-foldable PQ-surface has one degree of freedom (DoF), thus the change of its shape can be controlled by a single active R-joint.

It is well known [1, Theorem 3.2] that PQ-surfaces have a continuous flexion if and only if every  $(3 \times 3)$  substructure is isometrically deformable. Based on spherical kinematic geometry [2], a partial classification of rigid-foldable  $(3 \times 3)$  building blocks was obtained by Stachel and the author [3, 4, 5]. Inspired by this approach, Izmestiev [6] obtained a full classification of continuous flexible  $(3 \times 3)$  complexes.

Note that the rigid-foldability of PQ-surfaces is not a property of the extrinsic geometry but of the intrinsic one, which is determined by the corner angles of the planar quads. Nonetheless, certain classes of rigid-foldable PQ-surfaces, so-called V-hedra and T-hedra, allow for direct access to their spatial shape through the use

of control polylines. Due to this intuitive design methods these classes, which were originally introduced by Sauer and Graf [7] in 1931, recently attracted attention in the context of transformable design (see [8, 9, 10] and the references therein). These T-hedra and V-hedra (and their related surfaces [8]) are more or less<sup>1</sup> the only known flexible PQ-surfaces which go beyond the rather abstract classification of  $(3 \times 3)$  building blocks [6].

For the paper at hand the *V-hedra*, which are discrete analogs of Voss<sup>2</sup> surfaces [13], are not of interest, in contrast to T-hedra. These discrete analogs of *profile-affine surfaces* [7, 14] are briefly recapped at the begin of the next section.

*Remark 1.* Jiang et al. [15] presented an optimization technique for an approximate penalization of isometrically deformed surfaces with planar quads. The method's design space is restricted to PQ-surfaces which can be seen as discretizations of continuous flexible smooth surfaces (e.g. Voss surfaces, profile-affine surfaces).  $\diamond$

### 1.1 Motivation, Outline and Review

A *T-hedron* (also known as *discrete T-surface*) can be considered as a generalization of a discrete surface of revolution in such a way that the vertically aligned axis of rotation is not fixed but traces the so-called *prism polyline* on the base plane  $\tau_0$ , which is orthogonal to the axis direction. Moreover, the action does not need to be a pure rotation but can be combined with an axial dilatation. By applying this discrete kinematic generation iteratively to a *profile polyline* located in plane  $\pi_0$  through the initial axis  $q_0$ , a quad-surface with planar trapezoidal<sup>3</sup> faces is obtained. The polygonal path of the profile vertex located in the base plane is called *trajectory polyline*. Therefore, the complete geometric information of the T-hedron is encoded within three polylines (prism, profile, trajectory).

If only the profile polyline is replaced by a smooth profile curve, we end up with a so-called semi-discrete<sup>4</sup> T-surface.

Every vertical strips of a discrete (semi-discrete) T-surface is a patch of a discrete (smooth) cylinder due to its construction. From the projective point of view these cylinders are cones with their tips located on the ideal line of the base plane  $\tau_0$ . If we apply a projective transformation to the discrete (semi-discrete) T-surface we obtain a so-called discrete (semi-discrete) cone-net (cf. [16]) as each vertical strip turns into a conical patch. These cone-nets are special in the way that the tips of all cones are collinear [17, page 69]; therefore we call them *axial cone-nets*. For the illustration of a T-hedron and its projective transformation we refer to [16, Fig. 5].

<sup>1</sup> Beside them only some initial stitching solutions of different  $(3 \times 3)$  building blocks were presented in the literature [11, 12].

<sup>2</sup> The letter V stands for Voss in the nomenclature V-hedron.

<sup>3</sup> The letter T stands for trapezoidal in the nomenclature T-hedron.

<sup>4</sup> This is the semi-discretization of the vertical kind [9]. There is also a second one of the horizontal kind, but in the paper at hand the semi-discretization always refers to the vertical kind.

It is well known (e.g. [18]) that in general projective transformations only preserve infinitesimal flexions but not continuous ones. Thus we are aiming to determine the necessary and sufficient conditions for continuous flexibility of discrete (semi-discrete) axial cone-nets. In analogy to the notation introduced by Sauer and Graf [7] we abbreviate continuous flexible discrete cone-nets by the nomenclature C-hedra, which are eponymous for the contribution at hand structured as follows:

In Section 2 we determine the complete class of axial C-hedra by reducing it to the study of an overconstrained planar linkage (Section 2.1). The obtained result can also be used to construct their semi-discrete analogs (Section 2.2). Moreover, we identify a novel subclass of axial P-nets within the determined class of discrete (semi-discrete) axial cone-nets. In Section 3 we conclude the paper with a generalization of this subclass and an outlook to future research.

But before we plunge in medias res, we list all examples of discrete and semi-discrete axial cone-nets with a continuous flexion known to the author:

- By fixing the location of the axis (i.e. the prism polyline degenerates into a point) for the class of discrete and semi-discrete T-surfaces, we obtain the first family of known examples. This subclass of *stretch rotation surfaces* is of great importance as the complete set of T-surfaces<sup>5</sup> can be reconstructed from it by a *parallelism operation* (for detail please see [7, 10, 14, 19]).
- A further family of known examples originate from curved origami. A huge variety of origami shapes can be produced by using curved creases. But the question arise if a continuous folding motion exists towards the flat state that keeps the ruling layout<sup>6</sup> [21]. This so-called *rigid-ruling folding* is the curved-crease analogue of rigid-folding. A special family of curved origami possessing a rigid-ruling folding are conic crease patterns with reflecting rule lines [21], which constitute examples of semi-discrete axial cone-nets with a continuous flexion.

A discretization of these crease patterns was done in [22] under preservation of rigid-foldability, which results in a family of axial C-hedra. For the proof of this property a constructive approach was used in [22] based on a compatible series of planar linkages. We will stress this method in the next section to obtain the complete class of axial C-hedra.

## 2 Determination of axial C-hedra

For the determination of axial C-hedra it is sufficient to consider only three consecutive conical strips according to [1, Theorem 3.2] already mentioned in Section 1. The tips of the three involved discrete cones  $\Lambda_k$  are denoted by  $S_k$  for  $k = 1, 2, 3$  and are located on the axis  $q$  of the axial cone-net, which is assumed to be vertical<sup>7</sup>.

<sup>5</sup> With exception of translational T-surfaces, which are obtained if the axis goes to infinity.

<sup>6</sup> For origami shapes with only planar curved creases the answer was recently given in [20].

<sup>7</sup> As this is the usual setup [7, 14] for stretch-rotation surfaces, whose relation to the obtained results is stressed latter on.

## 2.1 The planar linkage $\mathcal{L}$

We consider the cuts of the cone-net by planes  $\pi_i$  (for  $i = 0, 1, \dots, p$  and  $p \geq 3$ ) containing the edges of  $\Lambda_k$  and the axis  $q$  (see Fig. 1). All the obtained planar cuts can then be rotated into the plane  $\pi_0$ . The resulting planar structure can be interpreted as a planar linkage  $\mathcal{L}$  which consists of  $6 + 3p$  systems and  $7 + 5p$  joints with 1-DoF. According to the formula of Grübler we get as degree of freedom for the linkage the value  $1 - p$ . But this linkage has to have an overconstrained mobility as the aimed continuous flexion of the three consecutive conical strips induces a 1-DoF motion to  $\mathcal{L}$ . In the following we study the necessary and sufficient conditions for  $\mathcal{L}$  to have an overconstrained 1-DoF motion.

Let us start by introducing the used notation and coordinatization. Similar to [9, 10, 19] we choose our Cartesian coordinate frame in a way that the  $z$ -axis coincide with  $q$  and that  $\pi_0$  equals the  $xz$ -plane. Moreover, we can assume that its origin coincides with  $S_2$  and that  $S_1$  is located on the positive part of the  $z$ -axis. In addition we can orient the  $x$ -axis in a way that  $A_0$  has a positive  $x$ -coordinate. This yields the following coordinatization for the points illustrated in Fig. 1:

$$S_1 := (0, 0, a)^T, \quad S_3 := (0, 0, b)^T, \quad A_i := (d_i, 0, z_i)^T, \quad B_i = v_i A_i, \quad (1)$$

with  $a \geq 0$ ,  $d_0 \geq 0$ . Further we can assume  $a \neq 0$  and  $b \neq 0$  to exclude the coincidence of adjacent cones, as the arrangement of two cones has always a trivial flexion. Moreover, we use the following notation of non-zero bar lengths:

$$s_i := \overline{S_2 A_i} > 0, \quad t_i := \overline{S_1 A_i} > 0, \quad u_i := \overline{S_3 B_i} > 0. \quad (2)$$

Therefore the length of the bar  $\overline{S_2 B_i} > 0$  is given by  $|v_i|s_i$  with  $v_i \neq 0$ . Now we can express the coordinates of  $A_i$  in dependence of  $s_i$ ,  $t_i$  and  $a$  as:

$$d_i = \frac{\sqrt{2a^2 s_i^2 + 2a^2 t_i^2 + 2s_i^2 t_i^2 - a^4 - s_i^4 - t_i^4}}{2a}, \quad z_i := \frac{a^2 + s_i^2 - t_i^2}{2a}. \quad (3)$$

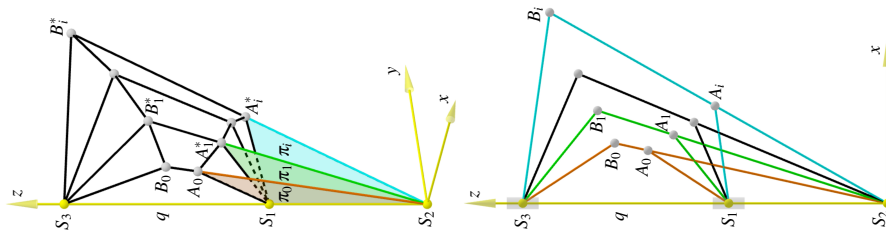


**Fig. 1** Schematic sketch of three consecutive conical strips of an axial C-hedra in an axonometric view (left) and the corresponding overconstrained planar linkage  $\mathcal{L}$  located in the  $xz$ -plane (right) where the sublinkages  $L_0$ ,  $L_1$  and  $L_i$  are highlighted in orange, green and blue, respectively. In order to save space the pictures are rotated by 90 degrees.



The idea is to use the slider associated with  $S_1$  (cf. Fig. 1) as active joint; i.e.  $a$  acts as parameter of the 1-DoF of  $\mathcal{L}$ . We can now compute the position of  $S_3$  in dependence of the sublinkage with index 0 of  $\mathcal{L}$ , which we call the initial sublinkage  $L_0$ . The equation  $\|B_0 - S_3\|^2 - u_0^2 = 0$  can be solved for  $b$  yielding following two solutions:

$$b_{\pm} := \frac{(a^2 + s_0^2 - t_0^2)v_0 \pm \sqrt{[a^4 - 2(s_0^2 + t_0^2)a^2 + (s_0 - t_0)^2(s_0 + t_0)^2]v_0^2 + 4u_0^2a^2}}{2a}. \quad (4)$$

Using this  $b_{\pm}$  value we can compute  $\|B_j - S_3\|^2 - u_j^2 = 0$  for any  $j \in \{1, \dots, p\}$  yielding the expression  $W_{j\pm}$ . Next we get rid of the square root of Eq. (4) in  $W_{j\pm}$  by an appropriate rearrangement and a subsequent squaring. The resulting expression<sup>8</sup> of the form  $f_j a^4 + g_j a^2 + h_j = 0$  has to be fulfilled independent of the motion parameter  $a$ . Therefore the coefficients  $f_j, g_j, h_j$ , which are given in detail in Appendix A, have to vanish. The solutions of the resulting system of equations  $f_j = g_j = h_j = 0$ , obtained by a detailed discussion of cases done in Appendix A, are summarized in the following theorem:

**Theorem 1.** *The linkage  $\mathcal{L}$  has an overconstrained 1-DoF mobility if and only if each sublinkage with index  $j$  for  $j \in \{1, \dots, p\}$  belongs to one of the following cases defined by the initial linkage  $L_0$ :*

1. *Central Scaling:*

- a. For  $v_0 = \frac{u_0}{t_0}$  and either  $z_0 \geq 0$  and  $b_+$  or  $z_0 \leq 0$  and  $b_-$ :  $v_j = \frac{u_0}{t_0}$ ,  $u_j = \frac{u_0 t_j}{t_0}$
- b. For  $v_0 = -\frac{u_0}{t_0}$  and either  $z_0 \leq 0$  and  $b_+$  or  $z_0 \geq 0$  and  $b_-$ :  $v_j = -\frac{u_0}{t_0}$ ,  $u_j = \frac{u_0 t_j}{t_0}$

2. *Perspective Collineation:*

- a. For  $v_0 = -\frac{u_0}{t_0}$  and either  $z_0 \geq 0$  and  $b_+$  or  $z_0 \leq 0$  and  $b_-$ :  
 $u_j = \frac{\sqrt{t_0 v_j (s_j^2 t_0 v_j + s_0^2 u_0 - t_0^2 u_0)}}{t_0}$ ,  $v_j = -\frac{u_0 (s_0^2 - t_0^2)}{t_0 (s_j^2 - t_j^2)}$
- b. For  $v_0 = \frac{u_0}{t_0}$  and either  $z_0 \leq 0$  and  $b_+$  or  $z_0 \geq 0$  and  $b_-$ :  
 $u_j = \frac{\sqrt{t_0 v_j (s_j^2 t_0 v_j - s_0^2 u_0 + t_0^2 u_0)}}{t_0}$ ,  $v_j = \frac{u_0 (s_0^2 - t_0^2)}{t_0 (s_j^2 - t_j^2)}$

3. *Central Perspectivity:*  $v_j = v_0$ ,  $u_j = \sqrt{s_j^2 v_0^2 - s_0^2 v_0^2 + u_0^2}$ ,  $t_j = \sqrt{s_j^2 - s_0^2 + t_0^2}$

Note that in case 3 the initial sublinkage can be arbitrary, in contrast to the cases 1 and 2, where the relation  $v_0 = \pm \frac{u_0}{t_0}$  of the *basic proportionality theorem* has to be fulfilled. If in case 3 this relation holds additionally true, then it also belongs to either case 1 or case 2 depending on the conditions implied by  $L_0$ . These are the only possible sublinkages belonging to two classes at the same time. Beside these linkages it is impossible that  $\mathcal{L}$  contains sublinkages of different classes, which can also be seen from the conditions implied by  $L_0$  (cf. Theorem 1).

On the other hand the set of sublinkages for the index  $j$  is only 1-dimensional for case 3 but 2-dimensional for the cases 1 and 2. This becomes more evident by the knowledge of the geometry of these cases, which is explained next.

<sup>8</sup> Is the same for  $W_{j-}$  and  $W_{j+}$ .

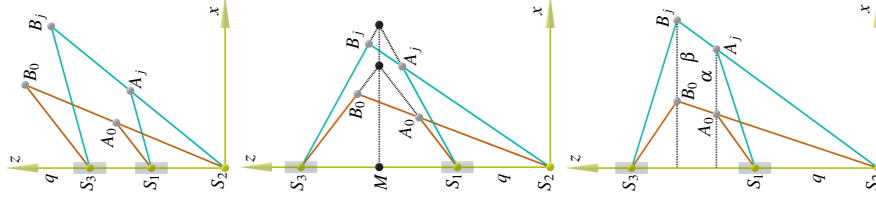


**Fig. 2** Illustration of the central scaling  $\sigma_1$  (left), perspective collineation  $\sigma_2$  (center) and central perspectivity  $\sigma_3$  (right), respectively. In order to save space the pictures are rotated by 90 degrees.

**Geometric interpretation of Theorem 1.** Based on the expression given in Theorem 1 it can easily be verified by direct computations that case  $k$  corresponds to the linear map  $\sigma_k$  for which  $\sigma_k(A_0) = B_0$  and  $\sigma_k(A_j) = B_j$  hold true for  $k \in \{1, 2, 3\}$ .

- ad 1: There exists a central scaling  $\sigma_1$  which maps  $S_1$  to  $S_3$  with center  $S_2$ .
- ad 2: There exists a perspective collineation  $\sigma_2$  which maps  $S_1$  to  $S_3$  with center  $S_2$  and the perpendicular to  $q$  through the midpoint  $M$  of  $S_1$  and  $S_3$  as axis.
- ad 3: We consider the two lines  $\alpha$  and  $\beta$  orthogonal to the axis  $q$  passing through the points  $A_0$  and  $B_0$ , respectively. There exists a central perspectivity  $\sigma_3$  with center  $S_2$  mapping points of  $\alpha$  to points of  $\beta$ .

The three mappings  $\sigma_1$ ,  $\sigma_2$  and  $\sigma_3$  are illustrated in in Fig. 2.

*Remark 2.* The limit cases of  $\sigma_k$  where at least one cone tip goes to infinity are discussed in Appendix B.  $\diamond$

## 2.2 Construction of continuous flexible (semi-)discrete cone-nets

Based on Theorem 1 we can construct three consecutive conical strips with a continuous flexibility. To do so, we assume that our initial linkage  $L_0$  is given as an input. As further input we construct a polyline  $A_0, A_1^*, \dots, A_p^*$  (cf. Fig. 1) with

$$A_j^* = (d_j \cos \phi_j, d_j \cos \phi_j, w_k)^T \quad \text{and} \quad \begin{cases} w_k = z_j & \text{for } k = 1, 2, \\ w_k = z_0 & \text{for } k = 3, \end{cases} \quad (5)$$

for case  $k$ . A rotation  $\delta_{-\phi_j}$  of  $A_j^*$  by the angle  $-\phi_j$  about the  $z$ -axis yields the missing input  $A_j$  of Eq. (1) for the construction of  $\mathcal{L}$ . Then we rotate the sublinkage  $L_j$  of  $\mathcal{L}$  back by the operation  $\delta_{\phi_j}$ . The obtained point  $B_j^* := \delta_{\phi_j}(B_j)$  completes the  $(3 \times p)$  C-hedral patch. In the case  $k = 3$  the patch belongs to a T-hedral stretch rotation surface (cf. Section 1.1). For  $k = 1, 2$  and  $p \geq 4$  we obtain a novel family of three consecutive conical strips with a continuous flexion up to the author's knowledge<sup>9</sup>.

<sup>9</sup> For  $p = 3$  the resulting  $(3 \times 3)$  patches have to be covered by the involved and quite abstract classification of Izmistiev [6] due to its claim of completeness.

*Remark 3.* If  $S_2$  goes to infinity (i.e.  $A_2$  degenerates into a cylinder), then we obtain for case 1 in the limit the translational case mentioned by Stachel [2, Sec. 1.2] and for case 2 the planar-symmetric case already known to Kokotsakis [23, § 18], respectively (see [2, Fig. 2] for the illustration of both limit cases).  $\diamond$

**Construction of the corresponding semi-discrete surface patches.** We can also apply the construction principle described above to a smooth input curve instead of a discrete one. In detail we replace the polyline  $A_0, A_1^*, \dots, A_p^*$  by a smooth curve  $\mathbf{a}^*(r)$  with parameter  $r \in [0; 1]$  and  $\mathbf{a}^*(0) = A_0$  for the respective case  $k$ ; i.e.

$$\mathbf{a}^*(r) = (d(r) \cos \phi(r), d(r) \cos \phi(r), w_k)^T \quad \text{with} \quad \begin{cases} w_k = z(r) & \text{for } k = 1, 2, \\ w_k = z_0 & \text{for } k = 3. \end{cases} \quad (6)$$

Then we apply again the rotation  $\delta_{-\phi(r)}$  to  $\mathbf{a}^*(r)$  to obtain  $\mathbf{a}(r)$ . The transformation of this curve with  $\sigma_k$  results in  $\mathbf{b}(r)$ . Finally,  $\mathbf{b}(r)$  is rotate back via  $\delta_{\phi(r)}$  to obtain  $\mathbf{b}^*(r)$  completing the continuous flexible arrangement of three smooth conical strips.

*Remark 4.* Instead of applying the three linear transformations  $\delta_{-\phi}$ ,  $\sigma_k$  and  $\delta_{\phi}$  consecutively in the discrete as well as semi-discrete setting, one could replace them directly by the spatial analog of the map  $\sigma_k$  for  $k \in \{1, 2, 3\}$ .  $\diamond$

By a subsequent combination of initial linkages of case 1 and case 2 we can generate novel discrete (semi-discrete) axial cone-nets of arbitrary dimensions with a continuous flexion. We call this new subclass discrete (semi-discrete) *axial P-nets* as for both cases 1 and 2 the proportion (P)  $v_0 = \pm \frac{u_0}{t_0}$  of the *intercept theorem* has to hold. Known special cases of these axial P-nets are the smooth and discrete conic crease patterns with reflecting rule lines (cf. [21, 22]).

### 3 Conclusion and future work

By using the already mentioned parallelism operation (cf. Section 1.1) one can even generalize the subclass of axial P-nets. The resulting general P-nets constitute a rich<sup>10</sup> novel class of continuous flexible discrete (semi-discrete) surfaces, which allow direct access to their spatial shapes by three control polylines (similar to T-surfaces). This intuitive method makes them suitable for transformable design tasks using interactive tools like the Rhino/Grasshopper plugin “Scutes” [8, 10]. The implementation of these general P-nets to “Scutes” is dedicated to future research as well as the parametrization of their isometric deformation required for coding. Further we plan a detailed discussion of their flexion limits, bifurcation configurations and possible tubular arrangements (in analogy to [9]).

An interesting open question remains towards the existence of non-axial C-hedra and their semi-discrete analogs.

<sup>10</sup> A simple parameter count reveals that the design space of a square patch has the same dimension as the corresponding one for T-hedra.

**Acknowledgements** The research is funded by project F77 (SFB “Advanced Computational Design”) of the Austrian Science Fund FWF. Moreover the author wants to thank Christian Müller for providing reference [17].

## References

1. Schief, W.K., Bobenko, A.I., Hoffmann, T.: On the integrability of infinitesimal and finite deformations of polyhedral surfaces. *Discrete Differential Geometry* (A.I. Bobenko et al. eds.), Oberwolfach Seminars **38**:67–93 (2008)
2. Stachel, H.: A kinematic approach to Kokotsakis meshes. *Computer Aided Geometric Design* **27**:428–437 (2010)
3. Nawratil, G., Stachel, H.: Composition of spherical four-bar-mechanisms. *New Trends in Mechanisms Science – Analysis and Design* (D. Pisla et al. eds.), pp. 99–106, Springer (2010)
4. Nawratil, G.: Reducible compositions of spherical four-bar linkages with a spherical coupler component. *Mechanism and Machine Theory* **46**(5):725–742 (2011)
5. Nawratil, G.: Reducible compositions of spherical four-bar linkages without a spherical coupler component. *Mechanism and Machine Theory* **49**:87–103 (2012)
6. Izmestiev, I.: Classification of flexible Kokotsakis polyhedra with quadrangular base. *International Mathematics Research Notices* **2017**(3):715–808 (2017)
7. Sauer, R., Graf, H.: Über Flächenverbiegung in Analogie zur Verknickung offener Facettenfläche. *Mathematische Annalen* **105**:499–535 (1931)
8. Kilian, M., Nawratil, G., Raffaelli, M., Rasoulzadeha, A., Sharifmoghaddama, K.: Interactive design of discrete (anti-)Voss nets and simulation of their rigid foldings. under review (2023)
9. Sharifmoghaddam, K., Maleczek, R., Nawratil, G.: Generalizing rigid-foldable tubular structures of T-hedral type. *Mechanics Research Communications* **132**:104151 (2023)
10. Sharifmoghaddam, K., Nawratil, G., Rasoulzadeh, A., Tervooren, J.: Using Flexible Trapezoidal Quad-Surfaces for Transformable Design. *Proc. of IASS Annual Symposia, Surrey Symposium: Transformable structures (IASS WG 15)*, pp. 1–13, IASS (2021)
11. Dieleman, P., Vasmel, N., Waitukaitis, S., van Hecke, M.: Jigsaw puzzle design of pluripotent origami. *Nature Physics* **16**(1):63–68 (2020)
12. He, Z., Guest, S.D.: On rigid origami II: Quadrilateral creased papers. *Proceedings of the Royal Society A* **476**(2237):20200020 (2020)
13. Voss, A.: Über diejenigen Flächen, auf denen geodätische Linien ein konjugiertes System bilden. *Münchener Berichte*, pp. 95–102 (1888)
14. Sauer, R.: *Differenzgeometrie*. Springer (1970)
15. Jiang, C., Wang, H., Inza, V.C., Dellinger, F., Rist, F., Wallner, J., Pottmann, H.: Using isometries for computational design and fabrication. *ACM Trans. Graphics* **40**(4):42 (2021)
16. Kilian, M., Müller, C., Tervooren, J.: Smooth and Discrete Cone-Nets. *Results in Mathematics* **78**:110 (2023)
17. Böklen, O.: *Analytische Geometrie des Raumes*. 2nd Edition, Cannstatt Verlag (1884)
18. Wegner, B.: On the projective invariance of shaky structures in Euclidean space. *Acta Mechanica* **53**:163–171 (1984)
19. Izmestiev, I., Rasoulzadeh, A., Tervooren, J.: Isometric Deformations of Discrete and Smooth T-surfaces. *arXiv:2302.08925* (2023)
20. Mundilova, K., Nawratil, G.: Rigid-Ruling Folding Compatibility of Planar Creases. (in preparation)
21. Demaine, E.D., Demaine, M.L., Huffman, D.A., Koschitz, D., Tachi, T.: Conic crease patterns with reflecting rule lines. *Origami<sup>7</sup>*, pp. 573–590, Tarquin (2018)
22. Demaine, E.D., Mundilova, K., Tachi, T.: Locally Flat and Rigidly Foldable Discretizations of Conic Crease Patterns with Reflecting Rule Lines. *Proc. of the 20th International Conference on Geometry and Graphics* (L.-Y. Cheng ed.), pp. 185–196, Springer (2023)
23. Kokotsakis, A.: Über bewegliche Polyeder. *Mathematische Annalen* **107**:627–647 (1932)

## Appendix A: Proof of Theorem 1

In the following we prove that the system of equations  $f_j = g_j = h_j = 0$  with

$$\begin{aligned}
f_j &:= (v_0 - v_j)[s_0^2 v_j v_0^2 - u_0^2 v_j + (u_j^2 - s_j^2 v_j^2) v_0], \\
g_j &:= (s_0^2 + s_j^2 - t_0^2 - t_j^2) v_0 s_j^2 v_j^3 + 2(s_0^2 u_0^2 - t_0^2 u_j^2) v_0^2 - (u_0 - u_j)^2 (u_0 + u_j)^2 \\
&\quad - s_j^4 v_j^4 - s_0^4 v_0^4 + 2[(t_0^2 - s_0^2) s_j^2 + s_0^2 t_j^2] v_0^2 v_j^2 + 2(s_j^2 u_j^2 - t_j^2 u_0^2) v_j^2 \\
&\quad + (s_0^2 v_0^2 - u_0^2 - u_j^2) (s_0^2 + s_j^2 - t_0^2 - t_j^2) v_0 v_j, \\
h_j &:= [(s_0^2 - t_0^2) v_0 u_j^2 - (s_0^2 - t_0^2) v_0 s_j^2 v_j^2 + (s_0^2 s_j^2 - s_0^2 t_j^2) v_0^2 v_j + (t_j^2 - s_j^2) u_0^2 v_j] \\
&\quad [(t_j^2 - s_j^2) v_j + v_0 (s_0^2 - t_0^2)],
\end{aligned} \tag{7}$$

has only the solutions listed in Theorem 1.

As  $t_j$  only appears in  $g_j$  and  $h_j$  we eliminate it from these two expressions by means of resultant; i.e.  $m_j := \text{Res}(h_j, g_j, t_j)$ . In a further step we compute  $\text{Res}(f_j, m_j, v_j)$  which factors into  $v_0^8 u_j^8 s_j^{16} F_-^{16} F_+^{16} G_-^6 G_+^6 H^{16}$  with

$$F_{\mp} = s_0 v_0 \mp u_0, \quad G_{\mp} = t_0 v_0 \mp u_0, \quad H = s_0^2 v_0^2 - s_j^2 v_0^2 - u_0^2 + u_j^2. \tag{8}$$

As the first three factors cannot vanish, we remain with the discussion of the factors given in Eq. (8).

- $F_{\mp} = 0$ : From this equation we can express  $v_0 = \pm \frac{u_0}{s_0}$ . Now the greatest common divisor (gcd) of  $f_j$  and  $m_j$  equals  $u_0(s_j v_j - u_j)(s_j v_j + u_j)$ . This expression cannot vanish without contradiction as the latter two factors imply  $b = 0$ .
- $G_- = 0, F_{\mp} \neq 0$ : From this equation we can express  $v_0 = \frac{u_0}{t_0}$ . Then the gcd of  $f_j$  and  $m_j$  equals  $u_0(t_0 v_j - u_0)(s_0^2 u_0 v_j - s_j^2 t_0 v_j^2 - t_0^2 u_0 v_j + t_0 u_j^2)$ . Thus we have to distinguish the following two cases:
  - ★  $v_j = \frac{u_0}{t_0}$ : Then the gcd of  $g_j$  and  $h_j$  equals  $(t_0 u_j + t_j u_0)(t_0 u_j - t_j u_0)$ . The first factor cannot vanish as all bar lengths are greater than zero. It can be seen that the second factor yields solution 1a after back substitution into  $W_{j\pm}$ .
  - ★  $u_j = \frac{\sqrt{t_0 v_j (s_j^2 t_0 v_j - s_0^2 u_0 + t_0^2 u_0)}}{t_0}$ : Now the gcd of  $g_j$  and  $h_j$  equals  $u_0^2 (s_0 - t_0)(s_0 + t_0)(t_0 t_j^2 v_j - s_j^2 t_0 v_j + s_0^2 u_0 - t_0^2 u_0)$ . The vanishing of the second and third factor yields  $F_{\mp} = 0$ , a contradiction. It can be seen that the last factor yields solution 2b after back substitution into  $W_{j\pm}$ .
- $G_+ = 0, F_{\mp} \neq 0$ : From this equation we can express  $v_0 = -\frac{u_0}{t_0}$ . Then the gcd of  $f_j$  and  $m_j$  equals  $u_0(t_0 v_j + u_0)(s_0^2 u_0 v_j + s_j^2 t_0 v_j^2 - t_0^2 u_0 v_j - t_0 u_j^2)$ . Thus we have to distinguish the following two cases:
  - ★  $v_j = -\frac{u_0}{t_0}$ : Then the gcd of  $g_j$  and  $h_j$  equals  $(t_0 u_j + t_j u_0)(t_0 u_j - t_j u_0)$ . The first factor cannot vanish as all bar lengths are greater than zero. It can be seen that the second factor yields solution 1b after back substitution into  $W_{j\pm}$ .

- ★  $u_j = \frac{\sqrt{t_0 v_j (s_j^2 t_0 v_j + s_0^2 u_0 - t_0^2 u_0)}}{t_0}$ : Now the gcd of  $g_j$  and  $h_j$  equals  $u_0^2 (s_0 - t_0)(s_0 + t_0)(s_j^2 t_0 v_j - t_0 t_j^2 v_j + s_0^2 u_0 - t_0^2 u_0)$ . The vanishing of the second and third factor yields  $F_{\mp} = 0$ , a contradiction. It can be seen that the last factor yields solution 2a after back substitution into  $W_{j\pm}$ .
- $H = 0, F_{\mp} G_{\mp} \neq 0$ : From this equation we can express  $u_j = \sqrt{s_j^2 v_0^2 - s_0^2 v_0^2 + u_0^2}$ . Now the gcd of  $f_j$  and  $m_j$  implies  $v_j = v_0$ . Then the gcd of  $g_j$  and  $h_j$  equals  $v_0^2 (s_0 v_j - u_0)(s_0 v_j + u_0)(s_0^2 - s_j^2 - t_0^2 + t_j^2)^2$ . The vanishing of the second and third factor yields  $F_{\mp} = 0$ , a contradiction. The last factor implies solution 3. This finishes the discussion of all cases.

## Appendix B: Discussion of limit cases

The maps  $\sigma_k$  of Section 2.1 are also well defined in the limit where  $S_2$  moves to infinity. Then the central scaling degenerates in a translation and the perspective collineation into a reflection (cf. Remark 3). We do not have to care about cases where either  $S_2$  and  $S_1$  or  $S_2$  and  $S_3$  are ideal points at the same time as in this case two adjacent cones coincide yielding a trivial flexion. Therefore we only have to consider the case where  $S_2$  is a finite point and  $S_1$  or/and  $S_3$  is/are ideal point/s.

- $\sigma_1$ : If only  $S_1$  (or  $S_3$ ) is an ideal point then all  $A_i$  (or all  $B_i$ ) are located at the line at infinity, thus the cone  $\Lambda_1$  (or  $\Lambda_3$ ) degenerates into the ideal plane, which is not feasible for the construction of a real PQ-mesh. However, we get a realizable configuration if both  $S_1$  and  $S_3$  are ideal points. In this case  $\sigma_1$  has to be defined by  $A_0 \mapsto B_0$ , as  $S_1 = S_3$  remains fixed under this mapping.
- $\sigma_2$ : In this case both points  $S_1$  and  $S_3$  have to be ideal points, but then we end up exactly with the same case discussed before.
- $\sigma_3$ : This map is also well-defined if  $S_1$  or/and  $S_3$  is/are ideal point/s.

*Remark 5.* Note that these limits cover all parabolic cases mentioned in [21, 22].  $\diamond$